1
2
3
4
5
6
7
8
9
10
11
12
13
14
15
16
17
18
19
20
21
22
23
24
25
26
27
28
29
30
31
32
33
34
35
36
37
38
39
40
41
42
43
44
45
46
47
48
49
50
51
52
53
54
55
56
57
58
59
60

Sintered-Silver Bonding of High-Temperature Piezoelectric Ceramic Sensors

Justine Billore, Stanislas Hascoët, Rémi Robutel, Cyril Buttay, *Senior Member, IEEE*, Jianfeng Li

***Abstract*—Silver sintering is used to bond five components together, in order to form a piezoelectric sensor. A description is provided of the preparation of these components, and of the manufacturing steps, which are carried out at a low temperature (280 °C).**

The resulting sensor assemblies are then characterized: cross-sectional views show that the silver layer has a very dense structure, with less than 1 % porosity, although further focused-ion beam investigations show that this porosity is closer to 15 %. The shear strength is approximately 30 MPa. The Young's modulus of the silver bondline is measured using nanoindentation, and is found to be comparable with that of bulk silver (56.6 GPa). Finally, a silver-sintered sensor is compared with a sensor bonded using conventional techniques, showing that an improvement in sensitivity by a factor of more than 3 is achieved.

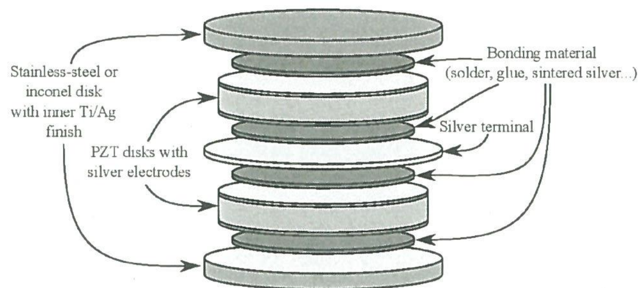

Fig. 1. Exploded view of a vibration sensor. Two vibration elements (PZT ceramics) are used in this device.

I. Introduction

VIBRATION SENSORS are used for a variety of applications. As an example, in oil and gas exploration, they are used to monitor the pressure and viscosity of the downhole fluids. These sensors are usually made from a stack of piezoelectric transducers and metal components. An example of such a stack is shown in Fig. 1. This (simplified) exploded view shows the the electro-active element of a larger sensor design, which is disclosed in patent [1]. The use of silver sintering to assemble this vibration sensor is protected by another patent [2]. The principle of such a sensor is to measure the resonant frequency of the piezoelectric elements, which can be used to determine various properties of the surrounding fluid (viscosity, density, etc.).

As wells become deeper, drilling tools are exposed to higher temperature (200 °C and more [3]). In the future, ambient downhole temperatures could even reach 600 °C for certain geothermal applications [4]. These conditions will require the use of high-temperature capable electronics and sensors.

In the case of vibration sensors, their assembly is an important issue since the various components used for the stack are either soldered or bonded together with adhesives. As the melting point of high temperature solders exceed the curie temperature of most piezoelectric ceramic (usually less than 330 °C [5]), a polarizing step is required following assembly of the stack. As an example, conventional High Melting Point (HMP) alloys require a process temperature of 380 °C. Although adhesives allow a simpler process to be used, they degrade rapidly at temperatures above 200 °C. In some applications with hermetic packaging, outgassing of the adhesive is also a concern, as it can lead to failure of the devices.

High-temperature power electronics are faced with the same type of challenge: how can semiconductor dies be bonded using a process that does not damage them, yet enables their long term operation (including thermal cycling) at temperatures above 200 °C? Several surveys [6], [7], [8] have been conducted in recent years, in an attempt to address this challenge.

For the assembly of vibration sensors, some technologies can be discarded immediately: all high temperature solders (AuGe, AuSn, etc.) require process temperatures exceeding 300 °C; silver-glass systems have a similar limitation, with a firing temperature generally greater than 600 °C [7]. Conductive adhesives were not investigated in detail in the aforementioned surveys, as their electrical and thermal conductivities are usually too low for power electronics applications. There are two remaining technologies that require a moderate process temperature, whilst offering a high-operating-temperature capability: Transient Liquid Phase Bonding (TLPB) and silver sintering.

TLPB (also refered to as SLID for Solid-Liquid InterDiffusion) consists in placing a thin layer of a low-melting point element, typically Sn or In (melting points at 232 and 157°C resp.), between two thicker layers of high melting temperature elements (typically Ag, Au or Cu, with melting points close to 1000°C). This stack is heated until the inner layer melts and diffuses through the solid layers, thereby forming an alloy with a higher melting point. The kinetics of this process are described in detail in [9]. An application for the assembly of stainless-steel substrates has been presented in [10]: the stack, produced with In for the inner layer and Ag for the solid layers, is heated to 190°C. A final melting temperature of 660 °C is achieved. a process temperature as low as 90 °C has been demonstrated in [11].

TLPB processes are usually based on thin metal layers (a few microns for the low melting point material), as this increases the bonding kinetics. However, when the parts to be

1
2
3
4
5
6
7
8
9
10
11
12
13
14
15
16
17
18
19
20
21
22
23
24
25
26
27
28
29
30
31
32
33
34
35
36
37
38
39
40
41
42
43
44
45
46
47
48
49
50
51
52
53
54
55
56
57
58
59
60

bonded have a high surface roughness, the thickness of the layer of low-melting material must be increased in order to ensure that any cavities are suitably filled. As a consequence, the high-temperature ("buffer") layers must also have a greater thickness. According to [12], a 1.5 μm surface roughness requires a 10 to 15 μm thick Au plating on the parts to be joined, which makes TLPB impractical for the bonding of rough surfaces. An alternative technique is that of Transient Liquid Phase Sintering (TLPS, [13]), in which the metal layers are replaced by small metal spheres that are able to fill the asperities of more complex bondlines.

Silver-sintering (melting point of Ag is 961 °C) is another technique allowing high-temperature assemblies to be bonded using a relatively low-temperature process (200–300 °C). A paste containing silver particles and various organic components (binder, thinner, etc. [14]) is stencil-printed between the parts to be bonded. A thermal cycle then causes the organic materials to evaporate, and allows the silver particles to be sintered, thus forming a solid silver layer interface.

This layer of pure silver has excellent thermal and electrical conductivities (429 W.m^{-1}.K^{-1} and 63.10^{6} S.m^{-1} respectively for bulk silver), as well as a higher reliability in the presence of thermal cycling, when compared to regular solders [15]. As a consequence, this technique has been intensively investigated, especially for power electronics applications. Silver pastes are now available from several manufacturers.

Although most power electronic systems are operated at moderate temperatures (below 200 °C), silver sintering has also been investigated for high temperature applications [16]. For example, in [17], is was observed is no noticeable drop occurs in the mechanical performance of a sintered-silver die attach following heat treatment at 300 °C for 400 h.

In this study, we describe the use of a silver sintering technique for the assembly of high-temperature vibration sensors. The manufacturing process is described in section II, and is characterized in section III. Finally, the results are discussed in section IV.

II. Assembly Process

The vibration sensor shown in Fig. 1 contains two piezoelectric elements (PZT ceramic), separated by a silver electrode, and is enclosed by metal washers at both ends. Two metal alloys (inconel 718, Ni: 50-55%, Cr: 17-21%, Fe: 24.6-13.2, Nb: 4.75-5.5 %, Mo: 2.8-3.3 %, Ti: 0.65-1.15 %, Al: 0.2-0.8 % and stainless-steel 316L, 64-66%, C: 0.02 %, Cr: 16-18 %, Ni: 11-13 %, Mo: 2 %) are selected for their ability to withstand corrosion in harsh environments, such as that experienced by downhole tools, or the turbines of aircraft engines.

A. Preparation of the parts

As the PZT disks (7.7 mm in diameter) are commonly supplied with silver electrodes (a silver paste, such as ref. 9910-C from ESL, or 7095 from Dupont, fired at high temperature), no special preparation was required for these disks.

A Ti/Ag (30-50nm/2-5μm) coating was applied (by sputtering) to one side of the metal disks (8.3 mm in diameter). Ti was used as an adhesive layer. The Ag finish is well matched to the silver sintering process.

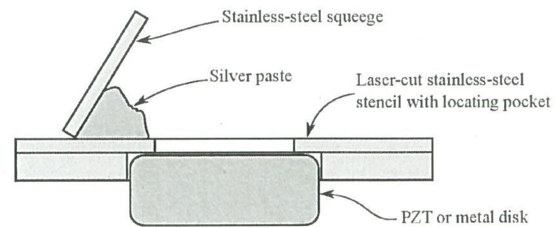

Fig. 2. Stencil printing of the silver paste, using a custom stencil with a centering pocket to ensure correct alignment.

A pure silver foil (Goodfellows, 99.9% purity, 50 μm thick, laminated) was used for the central electrode. This was cut to the desired shape using a CNC milling (CIF Technodrill).

All of the components were cleaned prior to assembly: 2 minutes in acetone (using an ultrasonic bath), 2 minutes in ethanol (ultrasonic bath), and were then dried using a nitrogen spray dryer.

B. Assembly

The layer of silver paste was applied using a manual stencil printing device, shown in Fig. 2: this uses a laser-cut, stainless-steel stencil with a locating pocket (the stencil is manufactured by bonding two-laser-cut foils). This stencil is placed over the component to process (either a PZT or a metal disk, as whown in Fig. 1), in order to control the dimensions and location of the layer of silver paste (Heræus ASP13106P2), which is applied using a stainless steel squeegee. The upper foil of the stencil has a thickness of 100 μm.

The printed parts are then left to dry on a hot plate, for 10 minutes at 100 °C. This results in a dry, non-tacky silver layer that does not spread during the pressure-assisted sintering process. After drying, the parts are stacked according to the arrangement shown in Fig. 1. A stainless-steel alignment jig [2] is used to ensure suitable coaxiality of the stack ($\pm$ 50 μm).

The jig is then placed between the plates of a heating press (described in [16]), and submitted to the following profile: firstly, the pressure plates are separated. A thermal cycle is initiated, with a 10 °C/min temperature ramp until 100 °C, followed by a 10 min plateau. The upper plate is then lowered and applied with a force of 196 N (corresponding to a pressure of 10 MPa in the silver layers). A second heating ramp (10 °C/min) is applied, to raise the temperature to 280 °C. This temperature is maintained for 30 min, following which the plates are separated and the system is allowed to cool down naturally. A study of these process parameters and their effects is given in [18]. In the same paper, differential scanning calorimetry (DSC) and thermogravimetric analysis (TGA) show that this temperature profile is sufficient to eliminate all of the volatile constituents from the paste. We thus consider that the final joint contains silver only. A cross-sectional view of this assembly is shown in Fig. 3

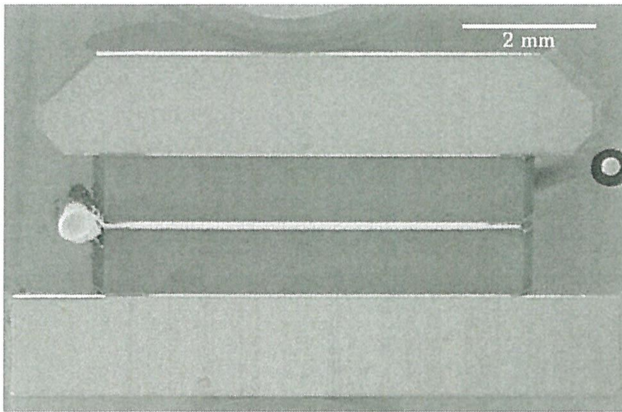

Fig. 3. Cross-sectional view of a sensor, with two metal disks (one, on top, with beveled edges, one on the bottom with square edges) and two PZT disks (smaller diameter, in the center). The two small circles (one on the left, one on the right) are cross-sectional views of the wire connected to the central electrode of the sensor.

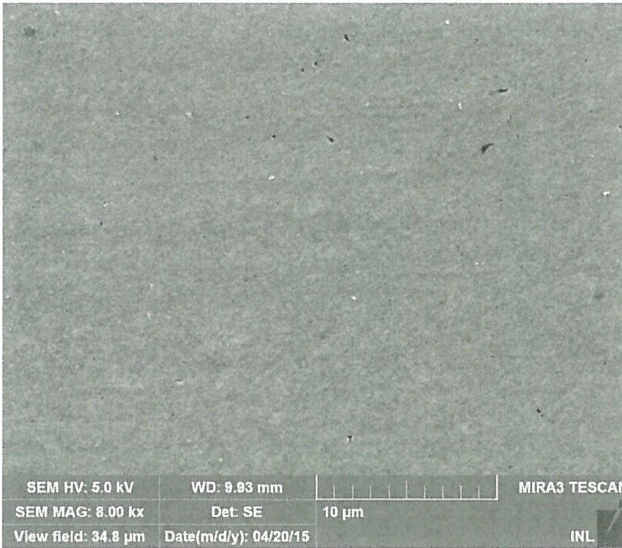

Fig. 4. SEM picture taken at the centre of the silver layer, showing very little porosity, characterized by a small number of sub-micronic pores.

III. Characterization

A. Microsections

After assembly, some of the samples were encapsulated in an acrylic resin (Buehler Varikleer), and cut using a low speed diamond saw (Escil Labcut 150). The surface was then polished (Presi Mecatech 334), using the following steps: P1200 SiC paper (1 min), followed by diamond slurries (9/3/1 μm, 3 min each) on hard clothes, and colloidal silica (1 min). The samples were then rinsed in de-ionised water and ethanol, and finally dried using a nitrogen spray dryer.

An electron microscope image of the silver layer, recorded near to the centre of the assembly is shown in Fig. 4. Optical microscope images of the silver layer, taken near to its edges, are shown at three different magnifications in Fig. 5. Note that this cross section corresponds to a simplified form of the full

TABLE I
Shear strength measured at different interfaces of the assembly. Tests performed at 22 °C.

Interface	sample #	Shear strength [MPa]
PZT/Inconel	1	34.4
	2	34.8
	3	50.0
PZT/Inox	4	33.2
	5	30.9
	6	31.9
PZT/silver foil	7	24.2
	8	47.7

stack shown in Fig. 1: here, only two metal disks, bonded with a single layer of silver, are shown.

As can be seen in Fig. 4, the apparent porosity of the silver layer is very low. We used image analysis software (imagej), to measure the porosity of various areas of this sample (excluding the edges of the silver layer), which was found to lie between 0,5 and 0,7 %. However, this measurement was also found to vary significantly from one sample to another: values as high as 4.4 % were observed in one of the assemblies.

In order to verify if this low apparent porosity is real, or if this is an artefact of the sample preparation (smearing of the silver during the mechanical polishing), one sample was prepared by Focused Ion Beam (FIB, Biophy Research, on a Tescan LYRA3 system). After cross section and mechanical polishing, a small ($\approx 10\times10\ \mu m^2$) window was opened in the exposed silver bondline using a beam of gallium ions. The result is visible in Fig. 6. It shows that the porosity is indeed much higher than observed after mechanical polishing. In the FIB-milled area, the porosity is measured at 15 %.

B. Mechanical characterization

One set of stacks was submitted to shear strength tests (using a Nordson Dage tester and a custom frame to hold the circular components), leading to the results shown in Table I. The significant scattering found in this data (from 24.2 to 50 MPa) is common with such mechanical tests, and can be explained by many factors, in particular small misalignments of the shear tool with respect to the circular components. Although the dataset represents a small number of measurements, we conclude that all of the stack interfaces are similar in strength.

One sample was used for a nanoindentation test. A microsection was produced, on which 20 indents were made at various locations on the silver joint. The corresponding force-displacement measurements are shown in Fig. 7. Each of these curves represents the loading of the inverter (penetration into the silver layer) up to a constant force of 40 mN, followed by unloading (removal). From the unloading section of the curve, it is possible to identify the value of Young's modulus for the sintered silver [19]. Using a Poisson's ratio of 0.37 for silver, the resulting Young's modulus in the direction of the indenter is found to be 56 $\pm$6 GPa, whereas the Young's modulus of pure silver is 76 GPa (Matweb).

Finally, some stacks were installed in the target system, in accordance with the method described by [1], and we measured the influence of the bonding technique on the electric

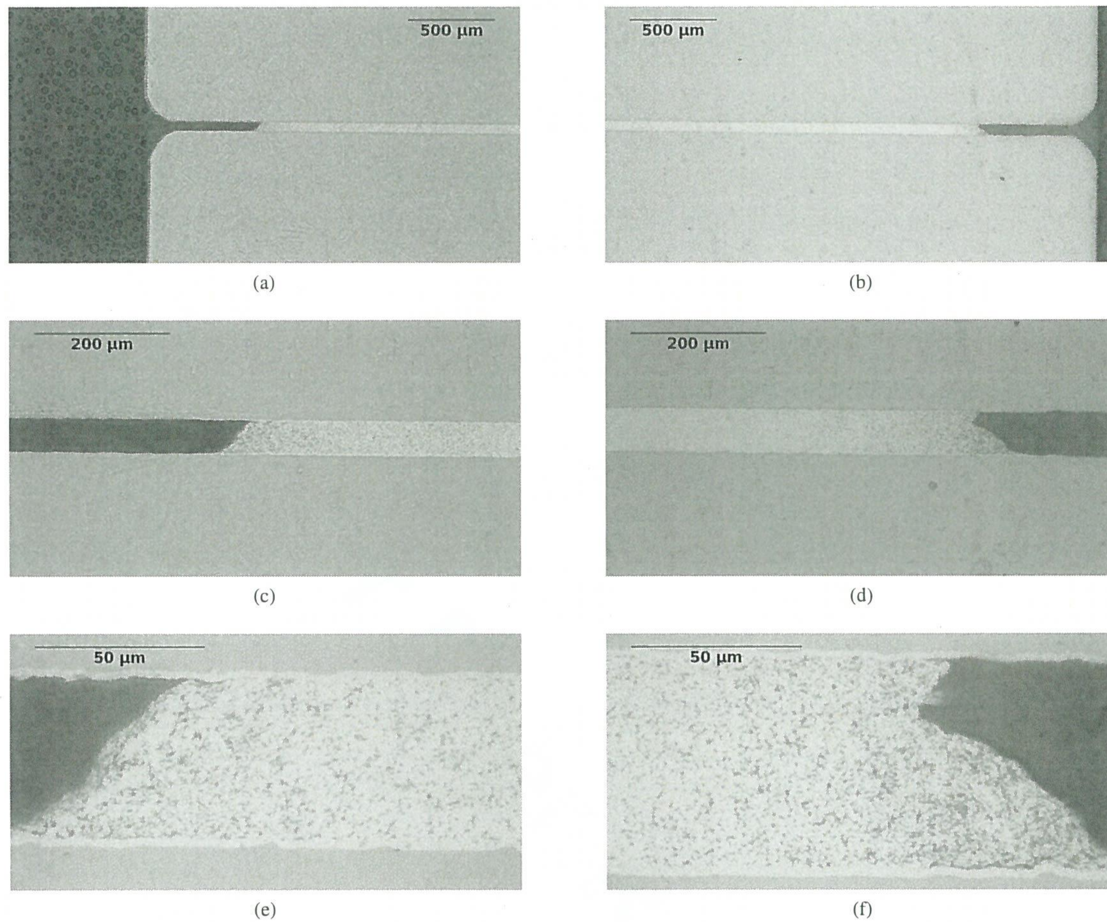

Fig. 5. Optical microscope view of the periphery of the sintered silver layer, showing a much higher porosity very close to the edges than in the center of the disks (full diameter = 8.3 mm). For these cross-sectional views, simplified stacks comprising only two metal disks were used. (a), (b): 5x enlargement, (c), (d): 20x enlargement, (e), (f): 100x enlargement and numerical enhancement of the depth of field.

signal. This is presented in Fig. 8. Initially, a burst of power was sent to the stack in order to generate some vibrations (actuator mode). Then (after t=1 ms), the stack was used as a sensor to measure the residual vibrations (in amplitude and frequency). These can be correlated with the density and viscosity of the surrounding fluid.

As shown in Fig. 8, when it is used in sensor mode (after t=1 ms), the silver-sintered stack generates a much larger signal ($>$ 3 times) than the glue-based stack ("reference assembly"). This reveals that the sensitivity of the silver-sintered sensor is significantly better than that of the reference device.

IV. Discussion

The low porosity of the silver layer is a key factor in this application: as the sensor is submitted to high temperatures and pressures during operation, a porous joint would gradually densify, leading to a change in the bondline thickness. This, in turn, would make the assembly shorter, and reduce its electro-mechanical coupling. Typical operating conditions for PZT ceramics correspond to applications involving a pre-load or pre-stress of several megapascals. Piezoelectric ceramics are strongly non-linear and under pre-load conditions, the piezoelectric coefficient (known as the d_{33} parameter) is close to its maximum and less sensitive to the temperature. The piezoelectric sensor's height stability is thus critical, since it is important to avoid any loss in sensitivity resulting from a change in operating conditions.

As a consequence, it is essential to achieve the lowest possible porosity in the joints of the piezoelectric stack. The microsections performed on the samples showed that their porosity is apparently very low (less than 1 %), but a FIB milling shows that the actual porosity is much higher (around 15 % on the area observed). As FIB milling can only be performed locally on a small area is not clear, however, if this porosity level is representative of that of the silver bondline. Indeed, the porosity level could change due to non-uniform application of the silver paste: as shown in Fig. 5 (in particular views (e) and (f), the bondline thickness varies across the width of the bond. From a total of 12 cross-sections, although the central bondline thickness was fairly consistent for a manual process (48 μm $\pm$ 9 μm, std. dev. 4.1 μm), bond parallelism discrepancies were observed. This could be

1
2
3
4
5
6
7
8
9
10
11
12
13
14
15
16
17
18
19
20
21
22
23
24
25
26
27
28
29
30
31
32
33
34
35
36
37
38
39
40
41
42
43
44
45
46
47
48
49
50
51
52
53
54
55
56
57
58
59
60

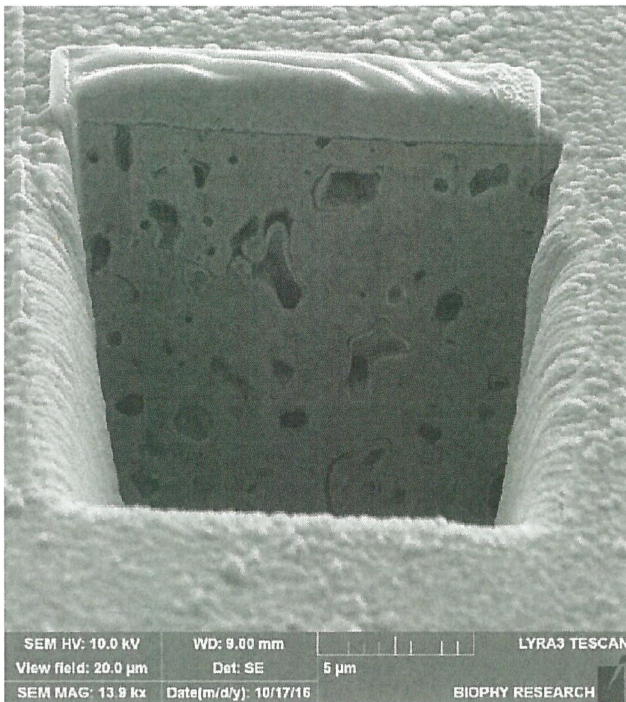

Fig. 6. Secondary electrons image of a FIB-milled area in the sintered silver layer of a sample (same as in Fig. 4). The apparent porosity is 15 %.

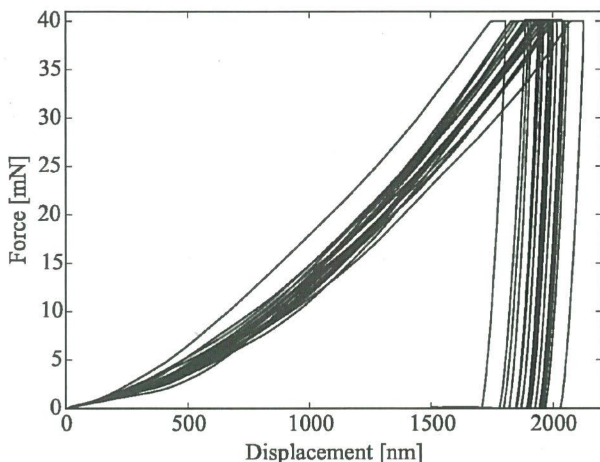

Fig. 7. Force-displacement graphs acquired using nano-indentation (Berkovitch indenter, 80 mN/min loading and unloading rate, 40 mN maximum load, acquisitions performed at 20 different locations).

improved through the use of a better stencil printing process: suitable control of paste rheology, speed and angle of the squeegee... and should allow more uniform silver deposits to be made. However, the relatively high porosity level observed with FIB preparation is consistent with the value of Young's modulus measured at the silver joint (56.6 GPa), which is lower than that of bulk silver (76 GPa). This difference could indeed be explained by a a presence of of 5-15 % porosity inside the joint [20]. Long term tests are ongoing to determine whether this porosity level is sufficiently low to remain stable

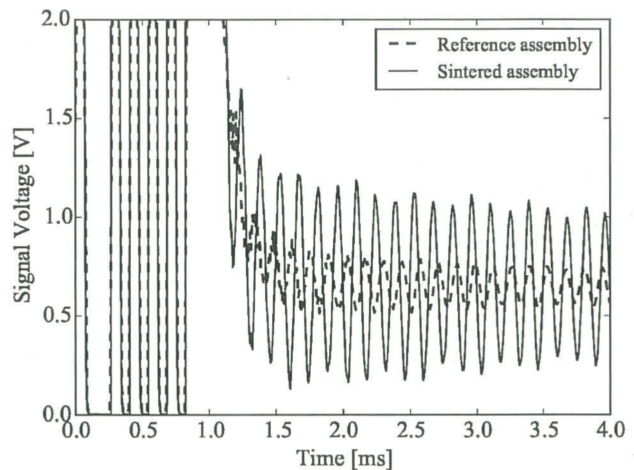

Fig. 8. Time-domain responses of two sensors produced using the reference and sintered assembly processes. These were acquired at 22 °C in water, with no load connected to the sensors.

during operation, or if a denser bondline is needed.

Although the shear strength results are not directly relevant for the sensor's application (since the stacks are submitted to compressive stress only), they demonstrate that all of the interfaces in the stack are strongly bonded. . The sputtered Ti/Ag layers on the metal disks also adhered wery well, allowing the stack to be interfaced with conventional stainless steel and inconel components.

A considerable improvement in electro-mechanical coupling is demonstrated in Fig. 8, and was confirmed by vibrometer measurements (not shown here). This enhanced performance can be attributed to the stiffer interface material (sintered silver instead of a softer silicone-based adhesive in the reference assembly), but also to the better quality of the bondline: very few voids can be found over the full length of the silver bondline.

From the point of view of practical applications, an additional advantage of silver sintering, when compared to organic glues is the reduced risk of outgassing following their installation: after the silver paste has dried, all of the organic constituents are removed [18], and only pure silver remains. Manufacturing of the sensors is facilitated: once the silver paste has been applied on the parts and dried, these can be handled with ease, with no risk of smearing the silver deposit. After drying, it is no longer necessary to assemble the parts immediately, as would be the case with a glue, and the sintering can be performed several hours (or perhaps even days) later. Finally, the press we used during this study could easily be replaced by a much simpler apparatus [21] which would allow the sintering to be performed in an oven (thus making it possible to manufacture several stacks in parallel). This approach allow the manufacturing process to be scaled up, for the production of a large number of sensors.

V. Conclusion

Silver sintering is becoming a well-accepted technology for the manufacture of power semiconductor dies attaches,

1
2
3
4
5
6
7
8
9
10
11
12
13
14
15
16
17
18
19
20
21
22
23
24
25
26
27
28
29
30
31
32
33
34
35
36
37
38
39
40
41
42
43
44
45
46
47
48
49
50
51
52
53
54
55
56
57
58
59
60

especially for high temperature applications. In this paper, we present the implementation of this technology for the manufacture of a piezoelectric sensor. This involves the use of a multilayer stack, comprising different materials, which is assembled in a single sintering step.

The manufacturing details are presented. The characterization of several manufactured units shows that the silver joint has a relatively low porosity, and a good adhesive properties. As a result, the complete sensor is considerably more sensitive than to currently used devices. Silver sintering is therefore a very attractive solution for the bonding of PZT actuators at relatively low temperatures,thus making it possible to avoid the risk of of de-polarization of these components.

REFERENCES

[1] F. Chaudoreille, A. Permuy, and E. Donzier, "Density and viscosity sensor," US Patent Patent US 7,874,199 B2, Jan. 25, 2011, uS Patent 7,874,199. [Online]. Available: https://www.google.fr/patents/US7874199

[2] R. Robutel, S. Hascoët, and N. Lacroix, "Fluid sensor with piezoelectric actuator and process for manufacturing the same," European Patent EP 2 846 159 A1, Mar. 11, 2015. [Online]. Available: https://data.epo.org/publication-server/rest/v1.0/publication-dates/20150311/patents/EP2846159NWA1/document.pdf

[3] R. Beckwith, "Downhole Electronic Components: Achieving Performance Reliability," *JPT*, pp. 42–53, Aug. 2013.

[4] R. Ásmundsson, R. Normann, H. Lubotzki, and B. Livesay, "High Temperature Downhole Tools," International Partnership for Geothermal Technology (IPGT), White paper, 2012. [Online]. Available: http://internationalgeothermal.org/Working_Groups/Documents/FINAL\%20High\%20Temperature\%20Tools\%20working\%20group\%20White\%20Paper.\%20August\%202012.pdf

[5] S. Zhang, R. Xia, L. Lebrun, D. Anderson, and T. R. Shrout, "Piezoelectric materials for high power, high temperature applications," *Materials Letters*, vol. 59, no. 27, pp. 3471–3475, 2005. [Online]. Available: http://www.sciencedirect.com/science/article/pii/S0167577X05005951

[6] L. Coppola, D. Huff, F. Wang, R. Burgos, and D. Boroyevich, "Survey on High-Temperature Packaging Materials for SiC-Based Power Electronics Modules," in *Power Electronics Specialists Conference, 2007. PESC 2007. IEEE*, Jun. 2007, pp. 2234–2240.

[7] V. Manikam and K. Y. Cheong, "Die Attach Materials for High Temperature Applications: A Review," *Components, Packaging and Manufacturing Technology, IEEE Transactions on*, vol. 1, no. 4, pp. 457–478, Apr. 2011.

[8] R. Khazaka, L. Mendizabal, D. Henry, and R. Hanna, "Survey of High-Temperature Reliability of Power Electronics Packaging Components," *Power Electronics, IEEE Transactions on*, vol. 30, no. 5, pp. 2456–2464, May 2015.

[9] W. Gale and D. Butts, "Transient liquid phase bonding," *Science and Technology of Welding and Joining*, vol. 9, no. 4, pp. 283–300, 2004. [Online]. Available: http://www.ingentaconnect.com/content/maney/stwj/2004/00000009/00000004/art00001

[10] C.-H. Sha and C. C. Lee, "Low-Temperature Bonding to 304 Stainless Steel for High-Temperature Electronic Packaging," *IEEE transactions on Components, Packaging and Manufacturing Technology*, vol. 1, no. 4, pp. 479–485, Apr. 2011.

[11] K. E. Aasmundtveit, T. A. V. Nguyen, and H.-V. Nguyen, "In–Bi Low-Temperature SLID Bonding," in *Electronics System Integration Technology Conference*, Grenoble, France, 2016.

[12] H.-V. Nguyen, T. Manh, T. Eggen, and K. E. Aasmundtveit, "Au-Sn Solid-Liquid Interdiffusion (SLID) Bonding For Mating Surfaces With High Roughness," in *Electronic System Integration Technology Conference (ESTC)*, Grenoble, France, 2016.

[13] H. Greve and F. P. McCluskey, "LT-TLPS Die Attach for High Temperature Electronic Packaging," in *Proceedings of the High Temperature Electronics Network (HiTEN)*. Oxford, UK: IMAPS, Jul. 2013, pp. 246–253.

[14] G. Bai, "Low-Temperature Sintering of Nanoscale Silver Paste for Semiconductor Device Interconnection," Ph.D. dissertation, Virginia Polytechnic Institute and State University, Blacksburg, Virginia, Oct. 2005. [Online]. Available: http://scholar.lib.vt.edu/theses/available/etd-10312005-163634/unrestricted/Dissertation-GBai05.pdf

[15] M. Knoerr, S. Kraft, and A. Schletz, "Reliability Assessment of Sintered Nano-Silver Die Attachment for Power Semiconductors," in *Proceedings of the 12th Electronics Packaging Technology Conference (EPTC)*. Singapore: IEEE, Dec. 2010, pp. 56–61.

[16] C. Buttay, A. Masson, J. Li, M. Johnson, M. Lazar, C. Raynaud, and H. Morel, "Die Attach of Power Devices Using Silver Sintering - Bonding Process Optimisation and Characterization," in *Proceedings of the High Temperature Electronics Network Conference (HiTEN 2011)*. Oxford, UK: IMAPS, Jul. 2011. [Online]. Available: https://hal.archives-ouvertes.fr/hal-00672619

[17] G.-Q. Lu, J. Calata, G. Lei, and X. Chen, "Low-temperature and pressureless sintering technology for high-performance and high-temperature interconnection of semiconductor devices," in *Thermal, Mechanical and Multi-Physics Simulation Experiments in Microelectronics and Micro-Systems, 2007. EuroSime 2007. International Conference on*. IEEE, 2007, pp. 1–5.

[18] S. Hascoët, C. Buttay, D. Planson, R. Chiriac, and A. Masson, "Pressureless Silver Sintering Die-Attach for SiC Power Devices," *Materials Science Forum*, vol. 740, pp. 851–854, 2012. [Online]. Available: https://hal.archives-ouvertes.fr/hal-00799893

[19] D. J. Shuman, A. L. Costa, and M. S. Andrade, "Calculating the elastic modulus from nanoindentation and microindentation reload curves," *Materials Characterization*, vol. 58, no. 4, pp. 380 – 389, 2007. [Online]. Available: http://www.sciencedirect.com/science/article/pii/S1044580306001860

[20] J. A. Choren, S. M. Heinrich, and M. B. Silver-Thorn, "Young's modulus and volume porosity relationships for additive manufacturing applications," *Journal of Materials Science*, vol. 48, no. 15, pp. 5103–5112, 2013. [Online]. Available: http://dx.doi.org/10.1007/s10853-013-7237-5

[21] L. Navarro, X. Perpiñà, P. Godignon, J. Montserrat, V. Banu, M. Vellvehi, and X. Jordà, "Thermo-mechanical assessment of die-attach materials for wide bandgap semiconductor devices and harsh environment applications," *IEEE transactions on Power Electronics*, vol. 99, p. 1, 2014.